

Exceptionally High Carrier Mobility in Hexagonal Diamond

Zirui He,^{1, 2} Shang-Peng Gao,^{1, 2, *} and Meng Chen^{2, †}

¹College of Smart Materials and Future Energy, Fudan University, Shanghai 200433, China

²Shanghai Advanced Silicon Technology Co., Ltd., Shanghai 201616, China

Hexagonal diamond (h-diamond), or Lonsdaleite, has been reported to be a wide-bandgap semiconductor with high thermal conductivity and hardness. Our *ab initio* calculations show that h-diamond has exceptionally high carrier mobility. Along xy and z directions, the hole mobilities at 300 K are 5631 and $5552 \text{ cm}^2 \text{V}^{-1} \text{s}^{-1}$, and the room-temperature electron mobilities are 11462 and $28464 \text{ cm}^2 \text{V}^{-1} \text{s}^{-1}$, respectively. These values are superior to the mobility of most known semiconductors including cubic diamond (c-diamond). The small effective masses in h-diamond, comparable to those in c-diamond, cannot explain the mobility difference between the two phases. For holes, scattering induced by transverse acoustic phonons is the predominant mechanism near room temperature in c-diamond, whereas considerably suppressed in d-diamond by selection rules. The high electron mobility in h-diamond can be attributed to the wavefunction at the conduction band minimum, which is extended and distributed primarily in the lattice interstitial, leading to weak coupling with scattering potentials. The temperature dependence of h-diamond is investigated as well, which deviates from the power-law relationship due to the significantly increased occupation of optical modes at elevated temperatures. Consequently, our findings reveal h-diamond as a promising high-mobility semiconductor, and elucidate the microscopic origin in terms of the carrier-phonon scattering mechanisms beyond conventional understandings based on simple parameters such as effective mass.

Diamond, long prized as a gemstone, is also regarded as the “ultimate” wide-bandgap semiconductor material because of its excellent physical properties [1]. While most semiconductors may show good performance in certain properties, they often face inherent limitations in other critical characteristics. For example, GaAs has high electron mobility yet low hole mobility and thermal conductivity [2]; β -Ga₂O₃ has an ultrawide bandgap and large breakdown field, whereas its carrier mobility and thermal conductivity are unsatisfactory [3]. In contrast, diamond offers a unique combination of a series of key properties, including its high carrier mobility, high thermal conductivity, ultra-wide bandgap, and high breakdown field [1]. These intrinsic characteristics position it at the frontier of future electronics operating under the most extreme conditions of high power, frequency, and temperature [4].

In addition to the well-known cubic structure, diamond can also crystallize in the hexagonal phase. Hexagonal diamond (h-diamond), also referred to as Lonsdaleite [5], was both discovered in meteorites [6] and experimentally synthesized [7] in the 1960s. In contrast to cubic diamond (c-diamond) with a stacking sequence of AB-CABC... along the $\langle 111 \rangle$ crystallographic direction, it exhibits the ABAB... stacking. Although far less explored than the well-known cubic phase, existing studies have shown that the properties of h-diamond are comparable to, or even superior to, those of c-diamond. For example, Pan *et al.* [8] have revealed a 58% higher indentation strength of h-diamond than that of its cubic counterpart. Regarding the lattice thermal conductivity, studies on h-diamond report scattered values [9–11],

which are approximately 20–30% lower than that of c-diamond, yet still considerably outperform most of the known materials.

In this work, motivated by the recent success in the experimental synthesis of large-scale samples [12], we thoroughly investigate the carrier mobility of h-diamond, which is a key property that affects charge transport in semiconductors. Based on fully *ab initio* calculations, our results reveal that its electron mobility significantly exceeds that of most known semiconductor materials. We also shed light on the physical origin of its high carrier mobilities for both electrons and holes, which provides useful guidance for the discovery and design of novel high-mobility materials.

The calculated carrier mobilities of both phases are shown in Fig. 1. For c-diamond, the room-temperature hole mobility (μ_h) and electron mobility (μ_e) are predicted to be 2543 and $2068 \text{ cm}^2 \text{V}^{-1} \text{s}^{-1}$, respectively, in good agreement with experimental values. The high mobilities of both carrier types overcome the limitation of most conventional semiconductors that only one carrier type (usually electrons) exhibits high mobility. Regarding h-diamond, its carrier mobilities are found to be much higher. At 300 K, the hole mobilities are $\mu_h^{\perp c} = 5631$ and $\mu_h^{\parallel c} = 5552 \text{ cm}^2 \text{V}^{-1} \text{s}^{-1}$, and the electron mobilities are $\mu_e^{\perp c} = 11462$ and $\mu_e^{\parallel c} = 28464 \text{ cm}^2 \text{V}^{-1} \text{s}^{-1}$, both of which are even superior to the typical values of most known high-hole-mobility semiconductors (*e.g.*, Ge, with $\mu_h = 1820 \text{ cm}^2 \text{V}^{-1} \text{s}^{-1}$ [13]) and high-electron-mobility semiconductors (*e.g.*, GaAs, with $\mu_e = 8900 \text{ cm}^2 \text{V}^{-1} \text{s}^{-1}$ [14]). While the predicted hole mobility agrees well with the result in Ref. 15, our calculated electron mobility significantly exceeds the reported value. We performed calculations using two different *ab initio* methods for cross-verification, and the results are in reasonable agreement

* gaosp@fudan.edu.cn

† mchen@ast.com.cn

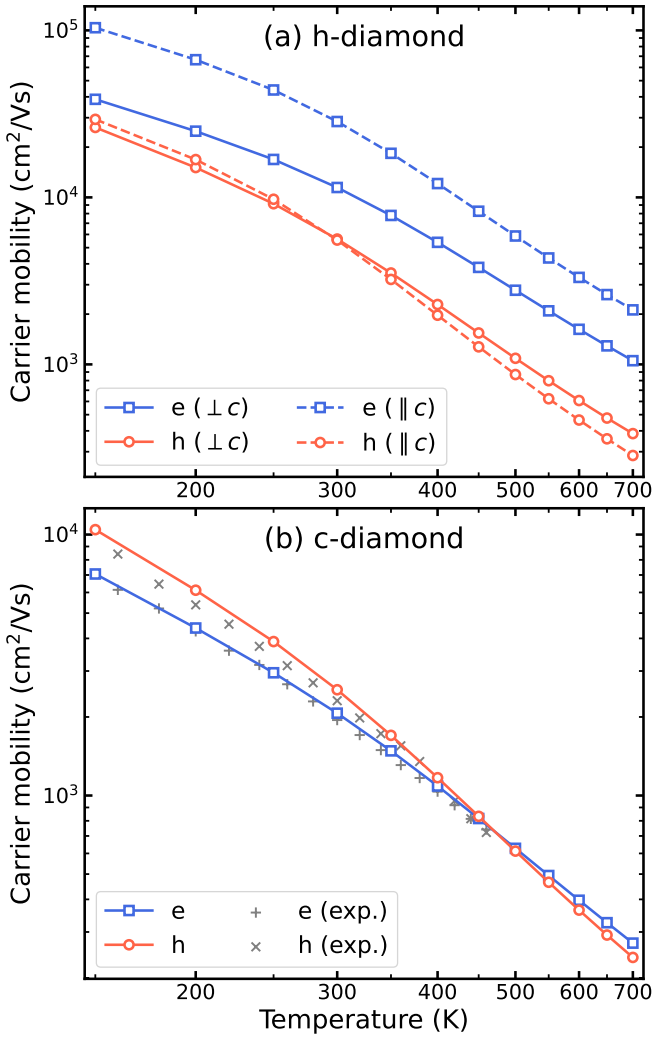


FIG. 1. Carrier mobilities of (a) h-diamond and (b) c-diamond, as functions of temperature. Experimental data are from Ref. 22.

[see Sec. S2 of Supplemental Material (SM) [16] for details], confirming the exceptional charge transport property of h-diamond. Since h-diamond has also been predicted to have a room-temperature thermal conductivity of nearly $2000 \text{ Wm}^{-1}\text{K}^{-1}$ [9, 11], it may outperform other novel semiconductor materials like BAs, which has drawn much attention in recent years due to its high ambipolar mobility (about $1600 \text{ cm}^2\text{V}^{-1}\text{s}^{-1}$) [17, 18] and high thermal conductivity (about $1300 \text{ Wm}^{-1}\text{K}^{-1}$) [19–21]. Additionally, our G_0W_0 calculation shows that h-diamond has a wide bandgap (4.55 eV according to our G_0W_0 calculation), and the molecular dynamics simulation at 1000 K indicates its high-temperature stability (see Sec. S3 in SM [16]). Therefore, h-diamond is expected as a promising candidate for applications in high-power and high-frequency electronics.

To pave the way for the high-temperature application of h-diamond, the temperature dependence of carrier mo-

bility is examined. Carrier mobility typically follows a power-law relationship with temperature, *i.e.*, $\mu \propto T^{-\alpha}$, if the scattering mechanism remains unchanged. However, as shown in Fig. 1(a), the temperature dependence of carrier mobility of h-diamond cannot be well described using the power law with a single exponent α within 150–700 K, suggesting a transition in the predominant scattering mechanism. Since h-diamond is a nonpolar semiconductor, deformation potential scattering is expected to play a crucial role, which can be induced by either acoustic or optical phonons. In order to elucidate the contributions of different phonon modes to carrier scattering, we define a function of phonon energy $\hbar\omega$ as

$$M(\hbar\omega) = \mu'(\hbar\omega)/\mu - 1, \quad (1)$$

where μ is the carrier mobility based on the self-energy time approximation [SERTA, see Eq. (S5) in SM [16]], with the scattering rate as

$$\tau_{n\mathbf{k}}^{-1} = \sum_{m\nu} \int_{\text{BZ}} \frac{d\mathbf{q}}{\Omega_{\text{BZ}}} \Gamma_{n\mathbf{k} \rightarrow m\mathbf{k} + \mathbf{q}}^{\nu}, \quad (2)$$

where $\Gamma_{n\mathbf{k} \rightarrow m\mathbf{k} + \mathbf{q}}^{\nu}$ is the transition rate from the initial state $n\mathbf{k}$ to the final state $m\mathbf{k} + \mathbf{q}$ by the phonon $\mathbf{q}\nu$. $\mu'(\hbar\omega)$ is analogous to μ , with the scattering rate replaced by

$$\tau_{n\mathbf{k}}^{-1}(\hbar\omega) = \sum_{m\nu} \int_{\text{BZ}} \frac{d\mathbf{q}}{\Omega_{\text{BZ}}} \Gamma_{n\mathbf{k} \rightarrow m\mathbf{k} + \mathbf{q}}^{\nu} [1 - g(\hbar\omega)], \quad (3)$$

where g is the Gaussian function $g(x) = \exp[-(x/a)^2]$, with a as the finite broadening. Consequently, $\mu'(\hbar\omega)$ is the carrier mobility that excludes scattering induced by phonons with an energy of $\hbar\omega$, and thus a larger $M(\hbar\omega)$ indicates a greater contribution of the corresponding phonons to limiting the mobility. As shown in Fig. 2, carrier scattering is mainly induced by phonons with an energy within two different ranges. The lower range is below 30 meV, indicating acoustic deformation potential (ADP) scattering. The higher range is between 138 and 160 meV, corresponding to optical modes. At 300 K, ADP is the predominant scattering mechanism. At higher temperatures, the relative contribution of optical phonons increases significantly, which dominate carrier-phonon scattering above about 400 K for holes and 450 K for electrons (see also Fig. S4 in SM [16]).

Given the same elemental composition and similar bonding characteristic of both phases, the reason for the much higher carrier mobility in h-diamond is of great interest. Mobility is usually associated with the carrier effective mass. A smaller effective mass typically indicates higher band velocities and a lower density of states (DOS), which give rise to faster carrier transport and reduced scattering phase space, respectively, thus leading to higher mobility. For example, it has been previously reported that the high hole mobility of c-diamond is mainly attributed to the small effective

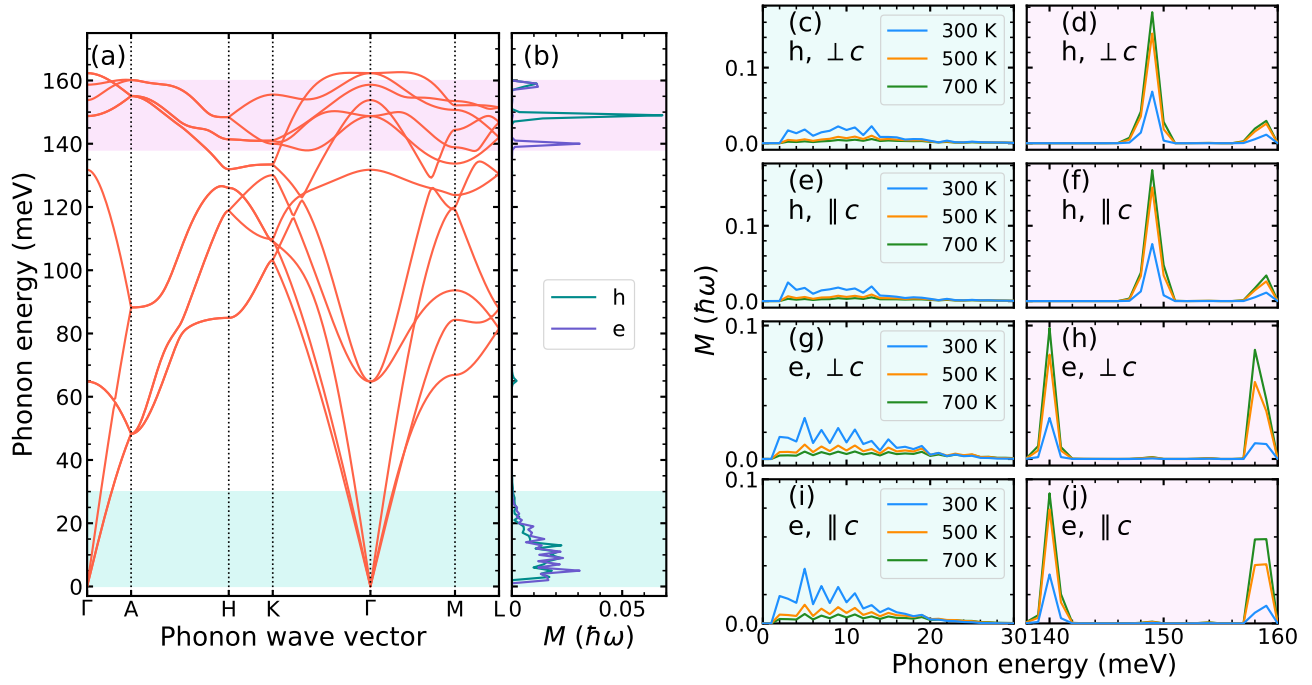


FIG. 2. (a) Phonon dispersion of h-diamond. (b) Calculated $M(\hbar\omega)$ for holes and electrons at 300 K. Two phonon frequency ranges characterized by significant acoustic-phonon scattering and optical-phonon scattering are highlighted with turquoise and violet, respectively. (c)–(j) Zoomed-in views of these two regions, with $M(\hbar\omega)$ evaluated at various temperatures.

mass [23]. For comparison, we calculate the “mobility effective masses” [24] to quantify the effect of band curvature on carrier mobility, as listed in Table I. And the DOS (per valley) is also evaluated for electronic states near band edges, as shown in Fig. S5 in SM [16]. Both quantities of h-diamond are comparable to those of c-diamond, supporting the small effective mass as an important contributor to the high mobility of h-diamond. However, it cannot explain the fact that the mobility in h-diamond is much higher than that in c-diamond, suggesting that other factors should play a crucial role. For example, one may attribute it to the differences in interband and intervalley scattering. For holes, the crystal-field splitting leads to a considerable energy gap (about 0.5 eV) between the valence band maximum (VBM) and the split-off hole (sh) band in h-diamond, which is likely to reduce the number of interband scattering channels. Regarding electrons, the conduction band minimum (CBM) of c-diamond at Δ has a larger multiplicity compared with that of h-diamond (CBM at K), which might cause enhanced intervalley scattering. Nevertheless, our calculations indicate that both effects have only minor contributions (see Sec. S4 in SM [16] for details), which will thus not be included in further discussion.

For holes in c-diamond, room-temperature mobility is predominantly limited by transverse acoustic (TA) phonons (see Fig. S6 in SM [16]), which agrees with previous study [23], and longitudinal acoustic (LA) phonons also play an appreciable role. These observations can be understood according to the selection rules (the notation

TABLE I. Calculated mobility effective masses, evaluated at 300 K and given in units of the electron rest mass. The definition is given in Eqs. (S6) and (S7) in SM [16].

Carrier	h-diamond			c-diamond
	$\perp c$	$\parallel c$	average	
Hole	0.472	0.682	0.586	0.489
Electron	0.462	0.261	0.368	0.373

for irreducible representations follows that of Ref. 25, see also Fig. S7 in SM [16]).

$$\begin{aligned} \langle 100 \rangle : \Gamma'_{25} \otimes \Delta'_2 &= \Delta_1 \oplus \Delta_5 = \text{TA} + \text{LA} + \text{TO} \\ \Gamma'_{25} \otimes \Delta_5 &= \Delta_1 \oplus \Delta'_1 \oplus \Delta_2 \oplus \Delta'_2 \oplus \Delta_5 \\ &= \text{TA} + \text{LA} + \text{TO} + \text{LO} \end{aligned} \quad (4)$$

$$\begin{aligned} \langle 110 \rangle : \Gamma'_{25} \otimes \Sigma_2 &= \Sigma_1 \oplus \Sigma_2 \oplus \Sigma_4 = \text{TA}_1 + \text{LA} + \text{TO} \\ \Gamma'_{25} \otimes \Sigma_1 &= \Sigma_1 \oplus \Sigma_2 \oplus \Sigma_3 = \text{TA}_2 + \text{LA} + \text{TO} + \text{LO} \end{aligned} \quad (5)$$

$$\langle 111 \rangle : \Gamma'_{25} \otimes \Lambda_3 = \Lambda_1 \oplus \Lambda_2 \oplus 2\Lambda_3 = \text{TA} + \text{LA} + \text{TO} + \text{LO} \quad (6)$$

Therefore, the symmetry places little restriction on acoustic modes. The scattering processes mediated by LA phonons are allowed for all these directions, and the TA modes are only partially forbidden.

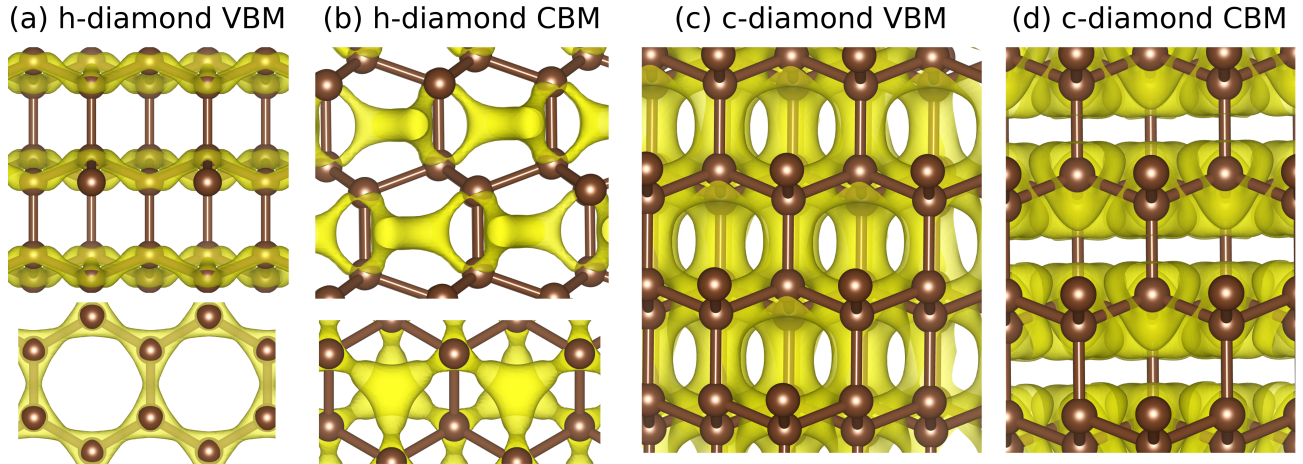


FIG. 3. Real-space distributions of charge density at VBM or CBM. The isosurfaces denote the values of (a) 3.5×10^{-4} , (b) 1.8×10^{-4} , (c) 7×10^{-4} , and (d) 1.08×10^{-3} a.u., respectively. Visualized using VESTA [26].

For h-diamond, the VBM is composed of p_x and p_y orbitals and has the Γ_5^+ symmetry, and the selection rules for in-plane scattering are

$$\Gamma_5^+ \otimes \Sigma_2 = \Sigma_1 \oplus \Sigma_3, \quad \Gamma_5^+ \otimes \Sigma_4 = \Sigma_1 \oplus \Sigma_3, \quad (7)$$

which originate from the symmetry of the Lonsdaleite structure. Since both the initial and final states are odd under the (0001) mirror symmetry, the phonons that are odd under it, such as the out-of-plane TA mode, are forbidden from inducing such transitions, thereby reducing the number of scattering channels. For comparison, although both h-diamond and wurtzite structures exhibit the AB stacking and have hexagonal symmetry, the compound nature of the latter breaks the (0001) mirror symmetry, and thus all phonons can induce such in-plane scattering in terms of symmetry. And the selection rule for scattering parallel to the c -axis is

$$\Gamma_5^+ \otimes \Delta_5 = \Delta_1 \oplus \Delta_2 \oplus \Delta_6, \quad (8)$$

indicating that both TA modes (Δ_5 symmetry) are forbidden. In conjunction with Eq. (7), it is found that the selection rules considerably suppress scattering in h-diamond caused by TA phonons, which predominantly limit hole mobility in c-diamond around room temperature. This could be a possible reason for the higher hole mobility in h-diamond.

Meanwhile, h-diamond has four atoms in the primitive cell, thereby introducing six additional phonon modes. To elucidate its effect on hole mobility, we first focus on the “high-energy” ($\hbar\omega \geq 132$ meV) modes. In c-diamond, the transverse optical (TO) modes are allowed by selection rules [Eqs. (4)–(6)] to induce scattering, while scattering mediated by longitudinal optical (LO) phonons is forbidden with the final states at the heavy-hole (hh) band [27] along $\langle 100 \rangle$ and $\langle 110 \rangle$ directions. This also explains the trend in Fig. S6 that TO phonons become dominant at elevated temperatures,

whereas LO phonons have a limited effect even at 700 K. In h-diamond, there are six optical branches within this range. Nevertheless, for both $\perp c$ and $\parallel c$ directions, only two TO modes (Δ_6 and Σ_1 symmetry) and one LO mode (Δ_1 and Σ_3 symmetry) are allowed by the selection rules [Eqs. (7) and (8)]. Hence, the optical phonons in the high-energy region lead to few additional scattering channels in h-diamond, except that the LO-induced scattering is less restricted by selection rules, which could explain the trend in Fig. 1 that the relative difference in hole mobility between the two phases becomes smaller at higher temperatures.

The “low-energy” ($\hbar\omega < 132$ meV) phonons in h-diamond along high-symmetry paths correspond to two interlayer shear modes and one interlayer breathing mode. For in-plane scattering, the shear vibrations are forbidden due to their odd parity under reflection across the (0001) plane [Eq. (7)]. Along the c -direction, the breathing mode (Δ_3 symmetry) is also forbidden [Eq. (8)]. In contrast, the breathing mode (for $\mathbf{q} \perp c$) and the shear modes (for $\mathbf{q} \parallel c$) are allowed to induce scattering, leading to non-zero matrix elements. These modes are characterized by shear or stretching vibrations of bonds parallel to the c -axis. As shown in Fig. 3, the p_x and p_y characteristic results in an in-plane distribution pattern of the charge density at VBM. Therefore, the spatial separation between the scattering potential and the charge distribution leads to weak carrier-phonon coupling in this regime.

On the other hand, the in-plane distribution of the charge density at VBM also gives rise to anisotropy of the hole effective mass, which is larger parallel to the c -axis. This is consistent with the calculated hole mobility based on SERTA, which is 23% lower along the z direction than that along the xy directions at 300 K. Nevertheless, the Boltzmann transport equation (BTE) mobility reveals a different trend, which is almost identical along three Cartesian directions at 300 K, with the

z -component 24% higher than that of SERTA; at lower temperatures, the z -component is even higher than the xy -components. This can be attributed to the weak scattering mediated by phonons with \mathbf{q} parallel to the c -axis. According to Eq. (8), both TA modes cannot induce scattering. The LA phonons, albeit allowed to mediate scattering, correspond to stretching vibrations of bonds parallel to the c -axis, thus resulting in suppressed scattering, similar to the case of interlayer shear and breathing modes discussed in the previous paragraph. In contrast, for $\mathbf{q} \parallel c$, scattering by the LA and in-plane TA modes is allowed, both of which incorporate vibrations of bonds parallel to the basal plane, thereby giving rise to considerable carrier-phonon coupling. Hence, the z -component of the band velocity of holes may be subject to little change due to scattering, leading to enhanced mobility along this direction, also explaining the underestimation of SERTA, which assumes complete loss of electronic momentum after each scattering process. At higher temperatures, the high-energy optical modes are activated, which incorporate in-plane opposite vibrations, and thus phonons with $\mathbf{q} \parallel c$ can also cause significant carrier-phonon coupling. Consequently, the hole mobility along the z direction becomes lower than the xy -components above 300 K. At 700 K, the z -component of BTE mobility is only 6% higher than its SERTA counterpart.

For electron scattering, the selection rules along three Cartesian directions are evaluated. In c-diamond, the constant-energy surfaces near the CBM [at Δ , with a Cartesian coordinate of $(u, 0, 0)$] manifest as ellipsoids. The selection rule for intravalley scattering along the principal axis is

$$\Delta_1 \otimes \Delta_1 = \Delta_1 = \text{LA}, \quad (9)$$

while that for scattering perpendicular to the principal axis is

$$\Delta_1 \otimes A_1 = \Delta_1 \oplus \Delta_2 \oplus \Delta_5 = \text{TA} + \text{LA} + \text{TO}, \quad (10)$$

where the Cartesian coordinate of the final state A is $(u, v, 0)$. In h-diamond (CBM at K), the selection rules are

$$x\text{-direction} : K_2^+ \otimes \Lambda_3 = \Lambda_1, \quad (11)$$

$$y\text{-direction} : K_2^+ \otimes B_1 = \Sigma_1 \oplus \Sigma_3, \quad (12)$$

$$z\text{-direction} : K_2^+ \otimes P_2 = \Delta_1 \oplus \Delta_4. \quad (13)$$

In both phases, LA phonons (Λ_1 , Δ_1 , and Σ_1 symmetry in h-diamond) are allowed to induce scattering, whereas transitions mediated by TA modes (Σ_3 , Σ_4 , Λ_3 , Λ_4 , and Δ_5 symmetry in h-diamond) are forbidden in specific directions. Compared with c-diamond, TA phonons in h-diamond are subject to stricter restrictions, which reduces the number of scattering channels, similar to the case of hole transport. Consequently, the TA-limited

electron mobility in c-diamond is approximately 2/3 of its actual mobility at 300 K, whereas in h-diamond, this ratio is below 30%. Nevertheless, the effect of optical phonons is more significant in h-diamond than in c-diamond, which partially offsets that of the suppressed TA-scattering. Therefore, the difference in the selection rules may be insufficient to account for the substantially higher electron mobility in h-diamond. Instead, the charge distribution provides a possible explanation. As shown in Fig. 3(b), the CBM state in h-diamond is composed of antibonding p_x and p_y orbitals, consistent with the D_{3h} point symmetry at the K points. The corresponding charge density exhibits an extended distribution within the interstitial regions of the lattice, giving rise to a small effective mass. Moreover, scattering potentials are primarily concentrated near the atoms and bonds (as nonpolar h-diamond lacks long-range Fröhlich interaction), leading to weak overlap with the electronic wavefunction at CBM, as shown in Fig. S8 in SM [16]. Such a “de-coupling” between electrons and phonons considerably decreases the values of matrix elements (Fig. S9 in SM [16]), thereby reducing the scattering rate, whereby playing an important role in the exceptionally high electron mobility of h-diamond.

In summary, the carrier mobilities in h-diamond and c-diamond are calculated using *ab initio* methods. At 300 K, the hole mobility perpendicular and parallel to the c -axis is 5631 and 5552 $\text{cm}^2\text{V}^{-1}\text{s}^{-1}$ in h-diamond, respectively, and the electron mobility along the two directions is 11462 and 28464 $\text{cm}^2\text{V}^{-1}\text{s}^{-1}$. These values are much higher than the mobility of c-diamond, in which the room-temperature hole and electron mobilities are 2543 and 2068 $\text{cm}^2\text{V}^{-1}\text{s}^{-1}$, respectively. In c-diamond, the ADP scattering mediated by TA phonons is the predominant scattering mechanism at room temperature, which is considerably suppressed in h-diamond by the selection rules. Although the interlayer shear and breathing modes provide additional scattering channels in h-diamond, they have weak interactions with the VBM state, which exhibits an in-plane distribution. At the CBM, the wavefunction of the CBM state is composed of antibonding p_x and p_y orbitals, which is extended and distributed mainly in the interstitial regions within the lattice, giving rise to spatial “de-coupling” with scattering potentials, resulting in high electron mobility. Other factors including effective mass have little contribution to the difference in carrier mobility between the two phases. We also show the temperature dependence of carrier mobility. At elevated temperatures, with the enhanced occupations of high-energy phonons, optical deformation potential scattering becomes the predominant mechanism, leading to a deviation from the power-law relationship. Our findings indicate that h-diamond is a promising candidate for high-frequency and high-speed applications. Furthermore, this work also offers a comprehensive picture of the carrier transport property of semiconductors. Although simple parameters, particularly effective mass, can usually provide a basic and straightforward

understanding of carrier mobility, other complicated factors, such as the symmetry and orbital component of the band extremum point, may also play a considerable role.

ACKNOWLEDGMENTS

This work was supported by research funds from Shanghai Advanced Silicon Technology Co., Ltd., and also the Natural Science Foundation of Shanghai (Grant No. 23ZR1403300).

[1] C. J. Wort and R. S. Balmer, Diamond as an electronic material, *Mater. Today* **11**, 22 (2008).

[2] J. S. Blakemore, Semiconducting and other major properties of gallium arsenide, *J. Appl. Phys.* **53**, R123 (1982).

[3] Z. Galazka, β -Ga₂O₃ for wide-bandgap electronics and optoelectronics, *Semicond. Sci. Technol.* **33**, 113001 (2018).

[4] S. Shikata, Single crystal diamond wafers for high power electronics, *Diam. Relat. Mater.* **65**, 168 (2016).

[5] C. Frondel and U. Marvin, Lonsdaleite, a hexagonal polymorph of diamond, *Nature (London)* **214**, 587 (1967).

[6] R. E. Hanneman, H. M. Strong, and F. P. Bundy, Hexagonal diamonds in meteorites: Implications, *Science* **155**, 995 (1967).

[7] F. P. Bundy and J. S. Kasper, Hexagonal diamond—a new form of carbon, *J. Chem. Phys.* **46**, 3437 (1967).

[8] Z. Pan, H. Sun, Y. Zhang, and C. Chen, Harder than diamond: Superior indentation strength of wurtzite BN and lonsdaleite, *Phys. Rev. Lett.* **102**, 055503 (2009).

[9] J. Zhang, Z. Zhao, M. Jiang, Y. Cheng, and G. Zhang, Thermal properties of hexagonal diamond: Machine learning potential and molecular dynamics study, *Phys. Rev. Mater.* **9**, 094603 (2025).

[10] L. Shi, X. Ma, Y. Zhong, M. Li, W. Yin, L. Yang, and X. He, Phonon thermal transport in diamond and lonsdaleite: A comparative study of empirical potentials, *Diam. Relat. Mater.* **120**, 108618 (2021).

[11] P. Chakraborty, G. Xiong, L. Cao, and Y. Wang, Lattice thermal transport in superhard hexagonal diamond and wurtzite boron nitride: A comparative study with cubic diamond and cubic boron nitride, *Carbon* **139**, 85 (2018).

[12] L. Yang, K. C. Lau, Z. Zeng, D. Zhang, H. Tang, B. Yan, G. Niu, H. Gou, Y. Yang, W. Yang, *et al.*, Synthesis of bulk hexagonal diamond, *Nature (London)* **644**, 370 (2025).

[13] F. J. Morin, Lattice-scattering mobility in germanium, *Phys. Rev.* **93**, 62 (1954).

[14] H. Hicks and D. Manley, High purity GaAs by liquid phase epitaxy, *Solid State Commun.* **7**, 1463 (1969).

[15] Y. Zheng, S. Lu, C. Chen, M. Jiang, X. Li, and X. Hu, Pure hexagonal diamond with symmetry-doping properties, *ACS Appl. Mater. Interfaces* **16**, 52674 (2024).

[16] See Supplemental Material at <http://link.aps.org/supplemental/10.1103/PhysRevB.XX.XXXXXX> for details of theoretical formulations, computational methods, high-temperature stability of h-diamond, effects of split-off hole band and intervalley scattering, and additional figures.

[17] S. Yue, F. Tian, X. Sui, M. Mohebinia, X. Wu, T. Tong, Z. Wang, B. Wu, Q. Zhang, Z. Ren, J. Bao, and X. Liu, High ambipolar mobility in cubic boron arsenide revealed by transient reflectivity microscopy, *Science* **377**, 433 (2022).

[18] J. Shin, G. A. Gamage, Z. Ding, K. Chen, F. Tian, X. Qian, J. Zhou, H. Lee, J. Zhou, L. Shi, T. Nguyen, F. Han, M. Li, D. Broido, A. Schmidt, Z. Ren, and G. Chen, High ambipolar mobility in cubic boron arsenide, *Science* **377**, 437 (2022).

[19] J. S. Kang, M. Li, H. Wu, H. Nguyen, and Y. Hu, Experimental observation of high thermal conductivity in boron arsenide, *Science* **361**, 575 (2018).

[20] S. Li, Q. Zheng, Y. Lv, X. Liu, X. Wang, P. Y. Huang, D. G. Cahill, and B. Lv, High thermal conductivity in cubic boron arsenide crystals, *Science* **361**, 579 (2018).

[21] F. Tian *et al.*, Unusual high thermal conductivity in boron arsenide bulk crystals, *Science* **361**, 582 (2018).

[22] M. Gabrysch, S. Majdi, D. J. Twitchen, and J. Isberg, Electron and hole drift velocity in chemical vapor deposition diamond, *J. Appl. Phys.* **109**, 063719 (2011).

[23] Q.-L. Yang, F.-C. Meng, W. Li, Z. Wang, H.-X. Deng, S.-H. Wei, F.-L. Ning, and J.-W. Luo, First-principles investigation of microscopic mechanisms underlying hole mobilities in diamond, silicon, and germanium, *Phys. Rev. B* **110**, 155203 (2024).

[24] S. Poncé, F. Macheda, E. R. Margine, N. Marzari, N. Bonini, and F. Giustino, First-principles predictions of Hall and drift mobilities in semiconductors, *Phys. Rev. Res.* **3**, 043022 (2021).

[25] M. S. Dresselhaus, G. Dresselhaus, and A. Jorio, *Group Theory: Application to the Physics of Condensed Matter* (Springer Berlin, Heidelberg, 2008).

[26] K. Momma and F. Izumi, *VESTA3* for three-dimensional visualization of crystal, volumetric and morphology data, *Journal of Applied Crystallography* **44**, 1272 (2011).

[27] It has been reported in Ref. 23 that the highest valence band along the $\langle 100 \rangle$ direction exhibits a light-hole-like characteristic. To avoid ambiguity, we refer to the three top valence bands in order of descending energy as the heavy-hole, light-hole, and split-off hole bands throughout this work.